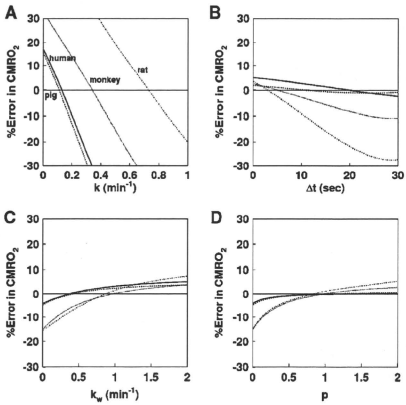

Figure 1 Error in $CMRO_2$ values due to errors in (**A**) k, (**B**) Δt, (**C**) k_w, and (**D**) p for assumed human, pig, monkey and rat. The same type of line indicates the same species. The percentage differences in the $CMRO_2$ values from the assumed true values (Table 1) were plotted as a function of the simulated value of k, Δt, k_w, and p.

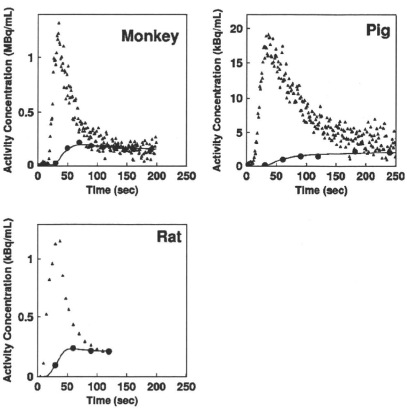

Figure 2 Representative comparison of the measured arterial whole blood and RW time activity curves for monkey, pig, and rat. Closed triangles and closed circles represent the measured whole blood and RW time activity curves, respectively. Estimated time activity curves by 4PF approach were also plotted in a solid line, and indicated a good agreement with the measured one.

optimized calibration protocol, k values were in a good agreement between 4PF and 1PF approaches. As shown in Figure 3, the regression analysis showed significant correlation for 21 animals including 6 monkeys, 3 pigs, and 12 rats ($P<0.001$), and there was no significant difference between the two variables. Figure 4 shows that k values calculated by the 1PF approach (at an optimized time) were in a good agreement with those calculated with the $BMRO_2$. Namely, the regression analysis showed significant correlation ($P<0.001$, $n=16$) and also that there was no significant difference between the two variables. Note that, in the $CMRO_2$ calculation by $BMRO_2$, k values were normalized according to the regression line shown in Figure 4. It should also be noted that calculated $CMRO_2$ values at the baseline shown in Table 3 were not significantly different among the four techniques. The average ($\pm$s.d.) values of obtained OEF were 0.53 ± 0.08, 0.52 ± 0.09, 0.54 ± 0.08, 0.54 ± 0.09, and 0.56 ± 0.04 from A–V difference, directly RW measured approach, 4PF, 1PF, and BM approaches, respectively. The Bland–Altman analysis of OEF values between from A–V difference and from others showed small over/underestimation, that is., with bias $\pm$ s.d. of -0.02 ± 0.09, 0.01 ± 0.07, 0.01 ± 0.08, and 0.02 ± 0.09, by direct RW, 4PF, 1PF, and BM approaches, respectively. Neither of the current methods (direct RW, 4PF, 1PF, and BM) was significantly different from A–V difference approach.

Discussion

Our study showed that the mathematical formula based on the physiologic model that reproduced the time-dependent concentration of RW in the arterial blood after a short-period inhalation of $^{15}O_2$ is indeed adequate. Our approach also simplified the procedures for sequential assessment of RW in $^{15}O_2$ inhalation PET studies, although previous approaches required frequent blood samples and centrifuges of each arterial blood sample. The present approach is an extension of a previous study by Iida *et al* (1993) and Huang *et al* (1991). It is essential if one intends to apply the rapid $^{15}O_2$ PET technique (Kudomi *et al*, 2005) to pharmacologic and physiologic stress studies on a wide range of species. Because the PET acquisition period can be prolonged > 3 mins, statistical accuracy can be significantly improved as compared with Ohta *et al* (1992) and other researchers (Fujita *et al*, 1999; Vafaee and Gjedde, 2000; Okazawa *et al*, 2001*a*, *b*; Yamauchi *et al*, 2003; Mintun *et al*, 2002), under which to avoid effects of RW, the data acquisition period was limited only to < 3 mins (Meyer *et al*, 1987; Ohta *et al*, 1992).

The present RW formula consists of three rate parameters of the production rate of RW in the arterial blood (k), and the forward and backward diffusion rate constants of RW between the blood and the peripheral tissues. The k was presumed to correspond to the oxygen metabolism in the total body system, $BMRO_2$, and was in fact shown to be

Table 2 Averaged values of k, Δt, k_w, and p for monkeys, pigs, rat, and human subjects under baseline condition

	Weight (kg)	k *(per min)*	*Δt (secs)*	k_w *(per min)*	p
Monkey	5.2 ± 0.8^a	0.34 ± 0.16^a	4.5 ± 1.4^a	0.98 ± 0.48	0.98 ± 0.30
Pig	38 ± 9^a	$0.11 \pm 0.02^{a,b}$	10.8 ± 1.8^a	0.83 ± 0.19	1.01 ± 0.26
Rat	0.30 ± 0.054^a	0.73 ± 0.16^a	2.9 ± 1.7^a	0.87 ± 0.30	0.83 ± 0.32
Human	58 ± 10^a	$0.129 \pm 0.023^{a,b}$	—	—	—

Monkey: $n = 6$; pig: $n = 3$; rat: $n = 12$; and human: $n = 231$. Measured values were obtained by 4PF for monkey, pig, rats, whereas those for human were obtained using data in a steady-state method.

[a]Denotes $P < 0.001$ for other species.

[b]Denotes that the difference was not significant in k between pig and human subjects.

Table 3 Values of k and $CMRO_2$ in the whole brain region for monkeys under physiologically baseline and stimulated conditions

ID	*Condition*	k *(per min)*			$CMRO_2$ *(mL/min per 100 g)*			
		4PF	*1PF*	$BMRO_2$	*Reference*	*4PF*	*1PF*	$BMRO_2$
1	BL	0.36	0.42	—	3.7	3.7	3.6	—
2	BL	0.62	0.66	1.24	3.0	3.3	3.4	3.4
3	BL (Dose of propofol)	0.32	0.39	0.83	3.0	3.1	3.0	2.9
4	BL	0.21	0.18	0.55	2.0	2.0	2.0	1.8
	8 mg/kg/h	—	0.30	0.69	—	—	—	—
	12 mg/kg/h	—	0.23	0.52	—	—	—	—
	16 mg/kg/h	—	0.16	0.40	—	—	—	—
5	BL	0.12	0.15	0.31	2.1	2.1	2.0	1.8
	5 mg/kg/h	—	0.15	0.32	—	—	—	—
	7 mg/kg/h	—	0.16	0.35	—	—	—	—
	10 mg/kg/h	—	0.18	0.36	—	—	—	—
	15 mg/kg/h ($PaCO_2$ level)	—	0.071	0.29	—	—	—	—
6	BL	0.43	0.46	0.95	2.8	3.1	3.0	3.3
	47 mm Hg	—	0.20	0.64	—	—	—	—
	33 mm Hg	—	0.21	0.46	—	—	—	—
	26 mm Hg	—	0.14	0.28	—	—	—	—
	42 mm Hg	—	0.33	0.82	—	—	—	—

4PF, four parameters fitting; 1PF, one parameter fitting; $BMRO_2$, total body metabolic rate of oxygen; BL, baseline condition.
Reference: RW TAC was obtained using measured RW data at a baseline condition in all monkeys ($n = 6$). No statistically significant differences were found in $CMRO_2$ between reference and other techniques.

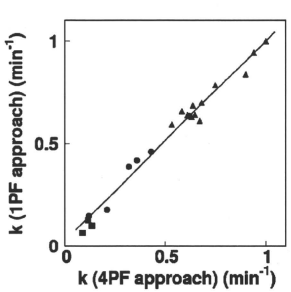

Figure 3 Comparison of the production rates of RW (k, per min) obtained by 4PF and those by 1PF. Squares, circles, and triangles correspond to pigs, monkeys, and rats, respectively. The regression line was $y = 0.97x + 0.026$ (per min) ($r = 0.98$).

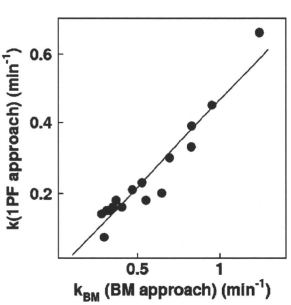

Figure 4 Comparison of the production rates of RW obtained by BM approach and those by 1PF approach in five monkeys at various anesthetic and $PaCO_2$ levels. The regression line was $y = 0.50x - 0.034$ (per min) ($r = 0.95$).

significantly correlated to $BMRO_2$, as measured from the trachea gas sampling (Figure 4). The latter two parameters (k_w and p) appeared to be consistent and did not differ across various species (Table 2). Also, change in those parameters was less sensitive in $CMRO_2$ (Figure 1). These findings suggest that the production of RW after inhalation of $^{15}O_2$ could be described only by a single parameter of k, as shown in Figure 3, although further studies are required to validate this because the method was only tested in a group with small number of subjects of particular physiologic situation (under anesthesia) and has not been applied to different populations. It is also important to note that this parameter (k) estimated from the $BMRO_2$ (i.e., BM approach) provided $CMRO_2$, which was consistent with the trachea gas samplings shown in Figure 4, and that the obtained OEF values by the approaches of 4PF, 1PF, and BM applied in the present study were not significantly different to that by A–V difference approach as revealed by Bland–Altman analysis.

The simulation study also showed that the most sensitive parameter in $CMRO_2$ was the RW production rate constant, k, followed by Δt. It was therefore suggested that k could be determined with a single blood sampling procedure using the 1PF approach, in which other parameter values were determined and fixed from results from the 4PF approach. It was further showed that k could be obtained from the BM approach as determined from oxygen concentration in the expiration gas. Both 1PF and BM approaches appeared to be robustly useful in $^{15}O_2$ PET for assessing quantitative $CMRO_2$ and CBF in clinical studies.

It is important to note that k varies significantly depending on the physiologic status even in the same species, as seen in Figure 4. According to the simulation study in Figure 1, this variation causes nonnegligible errors in $CMRO_2$, if a constant k is used. Changes in k from 0.1 to 0.6 per min causes errors in $CMRO_2$ of $\pm 30\%$ in anesthetized monkeys. Results from clinical studies, however, showed the variation in k being less. As shown in Table 2, k for clinical patients was 0.129 ± 0.023 per min, and the coefficient of variation was approximately 18%. Previous work by Huang *et al* (1991) also showed similar value with comparable variations, namely 0.131 ± 0.026 per min in six human subjects. These variations caused only $\pm 5\%$ errors in $CMRO_2$, according to the simulation shown in Figure 1. The small variation in k in clinical patients is attributed to the fact that all subjects were studied at a relatively stable condition without physiologic stimulation. However, careful attention is needed if one intends to scan the patients whose whole-body oxygen metabolism is largely changed from the baseline condition. For example, during several pharmacologically stressed (Wessen *et al*, 1997; Kaisti *et al*, 2003), exercise-induced physically stressed, and hyper- or hypothermia (Sakoh and Gjedde, 2003) conditions.

The simulation also showed that size of errors in $CMRO_2$ increased in smaller animals, where the value of k was larger. Recently, $CMRO_2$ as well as CBF have been measured in rats using a small animal PET scanner (Magata *et al*, 2003; Yee *et al*, 2006). Magata *et al* performed multiple blood samplings and plasma separation for multiple blood samples to estimate the RW in their experiment involving rats. The procedures were crucial, but have caused serious alterations of physiologic condition in heart pressure and heart rate due to large amount of blood samples for small animals. Our proposed simplified technique for estimating RW from a single blood sample or from $BMRO_2$, is essential for small animals to be able to maintain the physiologic status. The calculation of $CMRO_2$ also requires whole blood arterial TAC, which can be obtained from arterial blood samplings and could change the physiologic condition. However, such blood sampling could also be avoided by an arterial–venous bypass (Weber *et al*, 2002; Laforest *et al*, 2005), by placing a probe in femoral artery (Pain *et al*, 2004), or by a noninvasive method (Yee *et al*, 2006).

Mintun *et al* (1984) has proposed a simple procedure for RW correction based on a linear interpolation for the bolus $^{15}O_2$ inhalation 60-secs PET scan. As shown in Figure 2, the RW curve is not linear particularly in smaller animals, and a systematic error may be caused or scan duration is limited. Ohta *et al* (1992) and other investigators (Ohta *et al*, 1992; Fujita *et al*, 1999; Vafaee and Gjedde, 2000; Okazawa *et al*, 2001*a*, *b*; Yamauchi *et al*, 2003; Mintun *et al*, 2002), however, have used a technique which does not take into account the RW contribution. Only initial short-period data, namely the 3 mins after the bolus inhalation of $^{15}O_2$, were used in their approach, and thus estimated parameters suffered from statistical uncertainties. The present methodology to estimate RW in the arterial blood allows the prolongation of a PET acquisition period. The technique can also be applicable to the recently proposed sequential administration protocol of $^{15}O_2$ followed by $H_2^{15}O$ to estimate $CMRO_2$ and CBF simultaneously from a single session of a PET scan (Kudomi *et al*, 2005). This protocol, however, required a separation of a RW TAC from the whole blood TAC as showed recently (Kudomi *et al*, 2007).

The k_{BM} determined from the total body oxygen metabolism, namely the BM approach, was significantly greater than k obtained by the 4PF or the 1PF approach, by a factor 2, as shown in Figure 4. The reason is not clear, but partly attributed to the limitation of the simplified model. The body system consists of various organs which have different oxygen metabolism along with different circulation systems and with transit times. It is well known that the apparent rate constant defined with a simplified compartmental model could be underestimated as compared with an average of true rate constants, known as heterogeneity effects (Iida *et al*, 1989; Aston *et al*, 2002). This is, however, not essential.

Simply, linear correction could be applied to convert to the apparent k value as has been performed in this study. $CMRO_2$ values calculated using BM approach for the RW separation, were in good agreement with those determined with the direct measurement of RW as shown in Table 3.

The current method with modeling approach and simplified procedure provided consistent results in terms of time-dependent RW component, and consequently metabolic product of $^{15}O_2$ was separated from arterial whole blood for the $CMRO_2$ assessment in PET examination. The modeling approach to separate metabolite from authentic tracer has been showed previously for 6-[^{18}F]fluoro-L-dopa study (fdopa) (Huang *et al*, 1991). We expect that the modeling approach in conjunction with the simplified method showed in our study could be applied for various kinds of tracers, which require the separation of metabolic product such as fdopa. This approach enables us to assess parametric images for those tracers by eliminating the laborious procedures and by avoiding the amount of blood samplings, particularly for smaller animals.

In conclusion, the present RW model was feasible to reproduce RW TAC from a whole radioactivity concentration curve obtained after $^{15}O_2$ inhalation, and for a wide range of species. The simplified procedure to predict the RW TAC is of use to calculate $CMRO_2$ in smaller animals as well as clinical patients.

Acknowledgements

We acknowledge Mr N Ejima for operating the cyclotron and daily maintenance of CTI ECAT HR. We also gratefully thank Ms Atra Ardekani for her invaluable help on preparing the present paper. We also thank the staff of the Investigative Radiology, Research Institute, National Cardiovascular Center, especially, Dr T Inomata, Dr H Jino, Dr N Kawachi, and Dr T Zeniya for their assistance.

References

Aston JA, Cunningham VJ, Asselin MC, Hammers A, Evans AC, Gunn RN (2002) Positron emission tomography partial volume correction: estimation and algorithms. *J Cereb Blood Flow Metab* 22:1019–34

Eriksson L, Holte S, Bohm Chr, Kesselberg M, Hovander B (1988) Automated blood sampling system for positron emission tomography. *IEEE Trans Nucl Sci* 35:703–7

Eriksson L, Kanno I (1991) Blood sampling devices and measurements. *Med Prog Technol* 17:249–57

Fujita H, Kuwabara H, Reutens DC, Gjedde A (1999) Oxygen consumption of cerebral cortex fails to increase during continued vibrotactile stimulation. *J Cereb Blood Flow Metab* 19:266–71

Hayashi T, Watabe H, Kudomi N, Kim KM, Enmi J, Hayashida K, Iida H (2003) A theoretical model of oxygen delivery and metabolism for physiologic interpretation of quantitative cerebral blood flow and metabolic rate of oxygen. *J Cereb Blood Flow Metab* 23:1314–23

Hirano T, Minematsu K, Hasegawa Y, Tanaka Y, Hayashida K, Yamaguchi T (1994) Acetazolamide reactivity on ^{123}I-IMP single photon emission computed tomography in patients with major cerebral artery occlusive disease: correlation with positron emission tomography parameters. *J Cereb Blood Flow Metab* 14:763–70

Holden JE, Eriksson L, Roland PE, Stone-Elander S, Widen L, Kesselberg M (1988) Direct comparison of single-scan autoradiographic with multiple-scan least-squares fitting approaches to PET $CMRO_2$ estimation. *J Cereb Blood Flow Metab* 8:671–80

Huang SC, Barrio JR, Yu DC, Chen B, Grafton S, Melega WP, Hoffman JM, Satyamurthy N, Mazziotta JC, Phelps ME (1991) Modelling approach for separating blood time-activity curves in positron emission tomographic studies. *Phys Med Biol* 36:749–61

Iida H, Jones T, Miura S (1993) Modeling approach to eliminate the need to separate arterial plasma in oxygen-15 inhalation positron emission tomography. *J Nucl Med* 34:1333–40

Iida H, Kanno I, Miura S, Murakami M, Takahashi K, Uemura K (1989) A determination of the regional brain/blood partition coefficient of water using dynamic positron emission tomography. *J Cereb Blood Flow Metab* 9:874–85

Kaisti KK, Langsjo JW, Aalto S, Oikonen V, Sipila H, Teras M, Hinkka S, Metsahonkala L, Scheinin H (2003) Effects of sevoflurane, propofol, and adjunct nitrous oxide on regional cerebral blood flow, oxygen consumption, and blood volume in humans. *Anesthesiology* 99:603–13

Kudomi N, Choi C, Watabe H, Kim KM, Shidahara M, Ogawa M, Teramoto N, Sakamoto E, Iida H (2003) Development of a GSO detector assembly for a continuous blood sampling system. *IEEE Trans Nucl Sci* 50:70–3

Kudomi N, Hayashi T, Teramoto N, Watabe H, Kawachi N, Ohta Y, Kim KM, Iida H (2005) Rapid quantitative measurement of $CMRO_2$ and CBF by dual administration of ^{15}O-labeled oxygen and water during a single PET scan—a validation study and error analysis in anesthetized monkeys. *J Cereb Blood Flow Metab* 25:1209–24

Kudomi N, Watabe H, Hayashi T, Iida H (2007) Separation of input function for rapid measurement of quantitative $CMRO_2$ and CBF in a single PET scan with a dual tracer administration method. *Phys Med Biol* 52: 1893–908

Laforest R, Sharp TL, Engelbach JA, Fettig NM, Herrero P, Kim J, Lewis JS, Rowland DJ, Tai YC, Welch MJ (2005) Measurement of input functions in rodents: challenges and solutions. *Nucl Med Biol* 32:679–85

Lindstedt L, Schaeffer PJ (2002) Use of allometry in predicting anatomical and physiological parameters of mammals. *Lab Anim* 36:1–19

Magata Y, Temma T, Iida H, Ogawa M, Mukai T, Iida Y, Morimoto T, Konishi J, Saji H (2003) Development of injectable O-15 oxygen and estimation of rat OEF. *J Cereb Blood Flow Metab* 23:671–6

Meyer E, Tyler JL, Thompson CJ, Redies C, Diksic M, Hakim AM (1987) Estimation of cerebral oxygen utilization rate by single-bolus 15O2 inhalation and dynamic positron emission tomography. *J Cereb Blood Flow Metab* 7:403–14

Mintun MA, Raichle ME, Martin WR, Herscovitch P (1984) Brain oxygen utilization measured with O-15 radio-

tracers and positron emission tomography. *J Nucl Med* 25:177–87

Mintun MA, Vlassenko AG, Shulman GL, Snyder AZ (2002) Time-related increase of oxygen utilization in continuously activated human visual cortex. *Neuroimage* 16:531–7

Ohta S, Meyer E, Thompson CJ, Gjedde A (1992) Oxygen consumption of the living human brain measured after a single inhalation of positron emitting oxygen. *J Cereb Blood Flow Metab* 12:179–92

Okazawa H, Yamauchi H, Sugimoto K, Takahashi M, Toyoda H, Kishibe Y, Shio H (2001*a*) Quantitative comparison of the bolus and steady-state methods for measurement of cerebral perfusion and oxygen metabolism: positron emission tomography study using 15O-gas and water. *J Cereb Blood Flow Metab* 21:793–803

Okazawa H, Yamauchi H, Sugimoto K, Toyoda H, Kishibe Y, Takahashi M (2001*b*) Effects of acetazolamide on cerebral blood flow, blood volume, and oxygen metabolism: a positron emission tomography study with healthy volunteers. *J Cereb Blood Flow Metab* 21:1472–9

Pain F, Laniece P, Mastrippolito R, Gervais P, Hantraye P, Besret L (2004) Arterial input function measurement without blood sampling using a beta-microprobe in rats. *J Nucl Med* 45:1577–82

Sakoh M, Gjedde A (2003) Neuroprotection in hypothermia linked to redistribution of oxygen in brain. *Am J Physiol Heart Circ Physiol* 285:H17–25

Shidahara M, Watabe H, Kim KM, Oka H, Sago M, Hayashi T, Miyake Y, Ishida Y, Hayashida K, Nakamura T, Iida H (2002) Evaluation of a commercial PET tomograph-based system for the quantitative assessment of rCBF, rOEF and rCMRO2 by using sequential administration of 15O-labeled compounds. *Ann Nucl Med* 16:317–27

Temma T, Magata Y, Kuge Y, Shimonaka S, Sano K, Katada Y, Kawashima H, Mukai T, Watabe H, Iida H, Saji H (2006) Estimation of oxygen metabolism in a rat model of permanent ischemia using positron emission tomography with injectable^{15}O-O_2. *J Cereb Blood Flow Metab* 26:1577–83

Vafaee MS, Gjedde A (2000) Model of blood-brain transfer of oxygen explains nonlinear flow-metabolism coupling during stimulation of visual cortex. *J Cereb Blood Flow Metab* 20:747–54

Votaw JR, Shulman SD (1998) Performance evaluation of the Pico-Count flow-through detector for use in cerebral blood flow PET studies. *J Nucl Med* 39:509–15

Weber B, Burger C, Biro P, Buck A (2002) A femoral arteriovenous shunt facilitates arterial whole blood sampling in animals. *Eur J Nucl Med Mol Imaging* 29: 319–23

Wessen A, Widman M, Andersson J, Hartvig P, Valind S, Hetta J, Langstrom B (1997) A positron emission tomography study of cerebral blood flow and oxygen metabolism in healthy male volunteers anaesthetized with eltanolone. *Acta Anaesthesiol Scand* 41:1204–12

Yamauchi H, Okazawa H, Kishibe Y, Sugimoto K, Takahashi M (2003) The effect of acetazolamide on the changes of cerebral blood flow and oxygen metabolism during visual stimulation. *Neuroimage* 20:543–9

Yee SH, Lee K, Jerabek PA, Fox PT (2006) Quantitative measurement of oxygen metabolic rate in the rat brain using microPET imaging of briefly inhaled 15O-labelled oxygen gas. *Nucl Med Commun* 27:573–81

Eur J Nucl Med Mol Imaging (2009) 36:683–691
DOI 10.1007/s00259-008-0994-8

ORIGINAL ARTICLE

Parametric renal blood flow imaging using [^{15}O]H_2O and PET

Nobuyuki Kudomi · Niina Koivuviita · Kaisa E. Liukko · Vesa J. Oikonen · Tuula Tolvanen · Hidehiro Iida · Risto Tertti · Kaj Metsärinne · Patricia Iozzo · Pirjo Nuutila

Received: 14 May 2008 / Accepted: 17 October 2008 / Published online: 3 December 2008

Abstract
Purpose The quantitative assessment of renal blood flow (RBF) may help to understand the physiological basis of kidney function and allow an evaluation of pathophysiological events leading to vascular damage, such as renal arterial stenosis and chronic allograft nephropathy. The RBF may be quantified using PET with $H_2{}^{15}O$, although RBF studies that have been performed without theoretical evaluation have assumed the partition coefficient of water (p, ml/g) to be uniform over the whole region of renal tissue, and/or radioactivity from the vascular space (V_A. ml/ml) to be negligible. The aim of this study was to develop a method for calculating parametric images of RBF (K_1, k_2) as well as V_A without fixing the partition coefficient by the basis function method (BFM).
Methods The feasibility was tested in healthy subjects. A simulation study was performed to evaluate error sensitivities for possible error sources.
Results The experimental study showed that the quantitative accuracy of the present method was consistent with nonlinear least-squares fitting, i.e. $K_{1,BFM}=0.93K_{1,NLF}-0.11$ ml/min/g ($r=0.80$, $p<0.001$), $k_{2,BFM}=0.96k_{2,NLF}-0.13$ ml/min/g ($r=0.77$, $p<0.001$), and $V_{A,BFM}=0.92V_{A,NLF}-0.00$ ml/ml ($r=0.97$, $p<0.001$). Values of the Akaike information criterion from this fitting were the smallest for all subjects except two. The quality of parametric images obtained was acceptable.
Conclusion The simulation study suggested that delay and dispersion time constants should be estimated within an accuracy of 2 s. V_A and p cannot be neglected or fixed, and reliable measurement of even relative RBF values requires that V_A is fitted. This study showed the feasibility of measurement of RBF using PET with $H_2{}^{15}O$.

Keywords Positron emission tomography · Renal blood flow · Compartment model · Parametric image

N. Kudomi (✉) · K. E. Liukko · V. J. Oikonen · T. Tolvanen · P. Iozzo · P. Nuutila
Turku PET Centre, University of Turku,
P.O. Box 52, FIN-20521 Turku, Finland
e-mail: nobuyuki.kudomi@tyks.fi

N. Koivuviita · R. Tertti · K. Metsärinne · P. Nuutila
Department of Medicine, University of Turku,
Turku, Finland

H. Iida
Department of Investigative Radiology,
Advanced Medical-Engineering Center,
National Cardiovascular Center-Research Institute,
5-7-1, Fujishirodai,
Suita, Osaka 565-8565, Japan

P. Iozzo
Institute of Clinical Physiology, National Research Council,
56100 Pisa, Italy

Introduction

The quantitative assessment of renal blood flow (RBF) may help to understand the pathophysiological basis of kidney function and to evaluate pathophysiological events leading to vascular damage, such as renal arterial stenosis and chronic allograft nephropathy. The quantitative estimation of RBF by the use of $H_2{}^{15}O$ and dynamic PET has been developed and demonstrated by Nitzsche et al. [1]. The kinetic model of $H_2{}^{15}O$ is based on the assumptions that all activity is extracted by the parenchyma, extraction is very rapid, and tubular transport has not started or is insignificant at a level that does not influence the calculation of RBF [1–5]. With these assumptions, RBF has been estimated based on regions of interest (ROI) by the $H_2{}^{15}O$

dynamic PET approach [1, 3, 4]. Also, calculations to produce parametric images of RBF has been reported [5]. However, the quantitative computation of RBF has so far assumed that the blood/tissue partition coefficient of water (p, ml/g) is uniform for the whole region of renal tissue [3, 4], and/or that the contribution of radioactivity from the vascular space is negligible [5–7]. The influence on quantitative accuracy of these assumptions is unknown.

In previous studies RBF has been computed from the uptake rate (K_1, ml/min/g) [1–7]. Some studies also simultaneously computed the partition coefficient (p) [6, 7], and the apparent p values obtained ranged between 0.52 and 0.78 ml/g. From the published values of water content for tissue (76%) and blood (81%) [8], the p value can be physiologically determined as: p_{phys}=0.94 ml/g [9]. The much smaller apparent p value might be due to the tissue mixture (or a partial volume effect) [10, 11] because of the composite structure of the kidney. The effects of the tissue mixture affect mostly K_1 and not clearance rate (k_2 min^{-1}). Therefore the clearance rate of $H_2{}^{15}O$ (k_2 min^{-1}) multiplied by p_{phys} could be used for the calculation of blood flow rather than K_1 (ml/min/g) [11] when the effect of the tissue mixture is not negligible, although it is unknown how the glomerular filtration rate (GFR) additionally contribute to k_2. Thus, the influence of GFR on k_2 should be evaluated and allowed for in the computation of RBF.

The aim of this study was to develop a method to simultaneously calculate parametric images of K_1 and k_2 as well as the arterial blood volume (V_A, ml/ml). The feasibility in terms of quantitative accuracy and image quality of calculated images was experimentally tested in healthy subjects. GFR was measured in each subject to investigate how much it contributes to the clearance rate (k_2, min^{-1}). A simulation study was also performed to evaluate error sensitivities for possible error sources.

Materials and methods

Theory

The present formula was characterized by simultaneously estimating multiple parameters of uptake rate constant (K_1, ml/min/g) and clearance rate constant (k_2 ml/g) as well as activity concentration in the arterial vascular space (V_A, ml/ml). The kinetic model for $H_2{}^{15}O$ was based on a single-tissue compartment model as follows:

$$Ci(t) = (1 - V_A) \cdot K_1 \cdot A_w(t) \otimes e^{-k2 \cdot t} + V_A \cdot A_w(t) \qquad (1)$$

where $Ci(t)$ (Bq/ml) is radioactivity concentration in a voxel of PET image, $A_w(t)$ (Bq/ml) is the arterial input function, and ⊗ indicates the convolution integral.

In the present computation, we applied a basis function method (BFM) as introduced by Koeppe et al. [12] to compute the cerebral blood flow parametric image as well as the clearance rate constant simultaneously. Gunn et al. [13] applied this method to parametric imaging of both binding potential and the delivery of ligand relative to the reference region. The computation method has also been applied to myocardial blood flow studies to compute the uptake, clearance rates and blood volume [14, 15]. The BFM procedure for the present RBF computation is illustrated in Fig. 1. The BFM method enables parametric images to be computed by using linear least squares together with a discrete range of basis functions as the parameter value for k_2 incorporating the nonlinearity and covering the expected physiological range. The corresponding basis functions formed are:

$$F(k_2, t) = A_w(t) \otimes e^{-k2 \cdot t} \qquad (2)$$

For a physiologically reasonable range of k_2, i.e. $0 < k_2 < 15.0$ ml/min/g, 1,500 discrete values for k_2 were found to

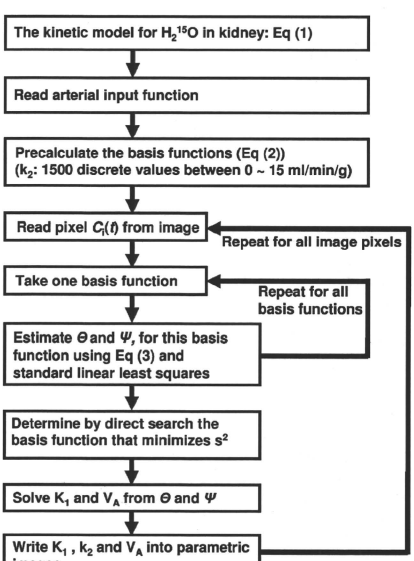

Fig. 1 Schematic diagram of the computation procedure by the BFM

be sufficient. Then Eq. 1 can be transformed for each basis function into a linear equation:

$$\begin{aligned} Ci(t) &= \Theta \cdot F(k_2, t) + \Psi \cdot A_w(t) \\ \Theta &= (1 - V_A) \cdot K_1 \\ \Psi &= V_A \end{aligned} \tag{3}$$

Hence for fixed values of k_2, the remaining two parameters Θ and Ψ can be estimated using the given basis function by standard linear least squares, and are represented as Θ_{k2} and Ψ_{k2}. The value k_2 for which the residual sum of squares

$$s(k_2)^2 = \sum_t \left(Ci(t) - \Theta_{k2} \cdot F(k_2, t) - \Psi_{k2} \cdot A_w(t)\right)^2 \tag{4}$$

is minimized is determined by a direct search, and associated parameter values for this solution (K_1, k_2, V_A) are obtained.

Subjects

Six healthy human subjects (the demographics are shown in Table 1) were studied under basal conditions and stimulation (after enalapril infusion) conditions. All subjects were nonsmokers and none of them was taking any medication. All subjects gave written informed consent. The study was approved by the Ethics Committee of the Hospital District of South-Western Finland, and was conducted in accordance with the Declaration of Helsinki as revised in 1966.

Table 1 Baseline characteristics of the six subjects studied

Characteristic	Mean±SD
Age (years)	58±5
Plasma creatinine (μmol/l)	85±10
Estimated GFR (ml/min)[a]	78±4
Weight (kg)	82.8±4.5
Body mass index (kg/m^2)	26.6±2.2
Blood pressure (mmHg)	
Systolic	136±11
Diastolic	82±4
Heart rate (min^{-1})	57±5
Fasting plasma total cholesterol (mmol/l)	5.3±1.0
Fasting plasma high density cholesterol (mmol/l)	1.5±0.4
Fasting plasma triglycerides (mmol/l)	1.2±0.4
Fasting plasma low density cholesterol (mmol/l)	3.2±0.8
Blood haemoglobin (g/l)	144±12
Fasting plasma glucose (mmol/l)	5.4±0.4

[a] Estimated according to the Modification of Diet in Renal Disease study equation.

PET experiments

PET was carried out in 2-D mode using a GE Advance scanner (GE Medical Systems, Milwaukee, WI). After a 300-s transmission scan, two scans were undertaken with injection of $H_2{}^{15}O$ (1.0 to 1.5 GBq) into the cephalic vein of the right forearm. The first scan was under resting conditions and the other was under stimulated conditions, namely 20 min after infusion of 0.5 mg enalapril. The scan protocol consisted of 20 frames over a total of 240 s (15×4 s, and 5×10 s). During PET scanning, blood was withdrawn continuously through a catheter inserted into the left radial artery using a peristaltic pump (Scanditronix, Uppsala, Sweden). Radioactivity concentrations in the blood were measured with a BGO coincidence monitor system. The detectors had been cross-calibrated to the PET scanner via an ion chamber [16]. GFR was also measured in each subject [17]. To obtain the PET equivalent flow ratio for GFR, a kidney weight of 300 g and a cortex ratio of 70% were assumed [8].

Data processing

Dynamic sinogram data were corrected for dead time in each frame in addition to detector normalization. Tomographic images were reconstructed from corrected sinogram data by the OSEM method using a Hann filter with a cut-off frequency of 4.6 mm. Attenuation correction was applied with the transmission data. A reconstructed image consisted 128×128×35 matrix size with a pixel size of 4.3×4.3 mm and 4.2 mm with 20 frames. Measured arterial blood time–activity curves (TAC) were calibrated to the PET scanner and corrected for the dispersion (τ=5 and 2.5 s for intrinsic and extrinsic, respectively) [18] and delay [19]. The corrected blood TAC was used as the input function.

A set of K_1, k_2 and V_A images was generated according to the BFM formula described above, using a set of dynamic reconstructed images and input function. Computations were programmed in C environment (gcc 3.2) on a Sun workstation (Solaris 10 Sun Fire 280R) with 4 GB of memory and two Sparcv9, 900-MHz CPUs.

Data analysis

A template ROI obtained by summing whole frames of a reconstructed dynamic image was drawn on an image of the whole region of each kidney (average ROI size for the all subjects was 153±43 cm^3). Also, a ROI was drawn on a region of high tracer accumulation on the summed image as an assumed cortical region. Functional values of K_1, k_2 and V_A were extracted from both ROIs, i.e. for the whole region and the cortical region, respectively. Data re shown individually or as means±SD. Student's paired t test was

used for comparisons between the physiological states and p values <0.05 were considered significant.

The ROI for the whole region was divided plane-by-plane into subregions of ten pixels each. The subregions were created by extracting pixels first from the horizontal direction and then from the vertical direction inside the whole ROI in each slice. Each subregion consisted of a single area with the same number of pixels. Functional values of K_1, k_2 and V_A were extracted from each subregion. Tissue TACs were also obtained for each subregion from corresponding dynamic images. The three parameters K_1, k_2 and V_A were estimated using the Eq. 1 and the input function fitted to the tissue TACs by the nonlinear least-squares fitting method (NLF, Gauss-Newton method). Functional values of K_1, k_2 and V_A from corresponding subregions were then compared between the methods. Regression analysis was performed.

The model relevancy introducing p and/or V_A into the computation was tested using the Akaike Information Criterion (AIC) [20]. The most appropriate model provides the smallest AIC. The tissue TACs from the subregions were fitted and AICs were computed for models with the three parameters K_1, k_2 and V_A, fixing p ($=K_1/k_2$) at 0.35 ml/g (mean value obtained in the present subjects), fixing V_A at 0 ml/ml, and fixing V_A at 0.15 ml/ml (mean value obtained in the present subjects).

Error analysis in the simulation

Error propagation from errors in the input function for the present BFM formula was analysed for two factors: delay and dispersion in arterial TAC. It is known that the measured arterial TAC is delayed and more dispersed relative to the true input TAC in the kidney because of the time for transit of blood through the peripheral artery and the catheter tube before reaching the detector [18, 19]. Calculations of RBF so far have employed a fixed partition coefficient (p, $=K_1/k_2$, ml/g) and/or assumed the blood volume (V_A, ml/ml) as negligible throughout the whole renal region and do not estimate it regionally. BFM formulae with a fixed value of p (BFM-pfix) and blood volume V_A (BFM-vfix) in addition to the present BFM formula, and the error in these formulae, were analysed.

A typical arterial input function obtained from the present PET study was used in the present simulation as the true input function. Applying this input function to the water kinetic model in Eq. 1, a tissue TAC was created assuming values for normal kidney tissue (K_1=2.0 ml/min/g, V_A=0.14 ml/g [5], and p=0.4 ml/g, corresponding to the estimated means in cortical region in all subjects in this study).

Time in the input function was shifted from −4 to 4 s to simulate the error sensitivity due to the error in the time delay, where a positive error represents an over-correction of the time delay. The input function was convoluted or deconvoluted with a simple exponential [18] by shifting the time constant from −4 to 4 s to simulate the error sensitivity due to error in dispersion correction, where a negative error represents under-correction, as described previously [18, 21]. Values of K_1 and k_2 were calculated using simulated input functions and the tissue TACs based on the BFM formula. Errors in these calculated K_1 and k_2 values are presented as percentage differences from the assumed values. Then, the value of p was varied from 0.3 to 0.5 ml/g and the tissue TAC was generated as above to simulate the error from the value of p in BFM-pfix formula. Also, the V_A value was varied from 0.0 to 0.4 ml/ml and the tissue TAC was generated to simulating the error from V_A in BFM-vfix formula. Then, K_1 and k_2 were calculated using the true input function and the created tissue TACs, assuming p=0.4 ml/g and V_A=0.0 ml/ml in the BFM-pfix and BFM-vfix formulae, respectively. Error in K_1 and k_2 values due to fixing p is presented as the percentage difference in K_1 and k_2 as a function of p. Error in K_1 and k_2 values due to neglecting V_A is presented as the percentage difference in K_1 and k_2 as a function of V_A. Also, K_1 and k_2 were computed with V_A fixed at 0.14 ml/ml in the BFM-vfix formula from the set of the tissue TACs, in which K_1 and p were fixed at 2.0 ml/min/g and 0.4 ml/g, respectively, and V_A was varied. The percentage difference in K_1 and k_2 between the two conditions, i.e. the initial (K_1=2.0 ml/min/g and V_A=0.14 ml/ml) and changed conditions (presented as ΔK_1 and Δk_2, respectively) is presented as a function of the percentage difference in the assumed V_A from 0.14 ml/ml (ΔV) to investigate the extents to which the change in K_1 and k_2 were estimated when K_1 and k_2 were computed in the BFM-vfix formula.

Results

Experiments

The relationships of the regional ROI values of K_1, k_2 and V_A between NLF and BFM are shown in Fig. 2. The regression lines obtained were $K_{1,BFM}=0.93K_{1,NLF}-0.11$ ml/min/g (r=0.80, p<0.001), $k_{2,BFM}=0.96k_{2,NLF}-0.13$ ml/min/g (r=0.77, p<0.001), and $V_{A,BFM}=0.92V_{A,NLF}-0.00$ ml/ml (r=0.97, p<0.001), where the subscripts show the methods used for calculating the parametric values; the slopes were not significantly different from unity.

The fitted curve by the present model estimating K_1, k_2 and V_A fitted better than the other two models fixing p ($=K_1/k_2$) or V_A. An example of fitted curves is shown in Fig. 3. Also, the AIC values from three parameter fitting were the smallest for all subjects except two values for two

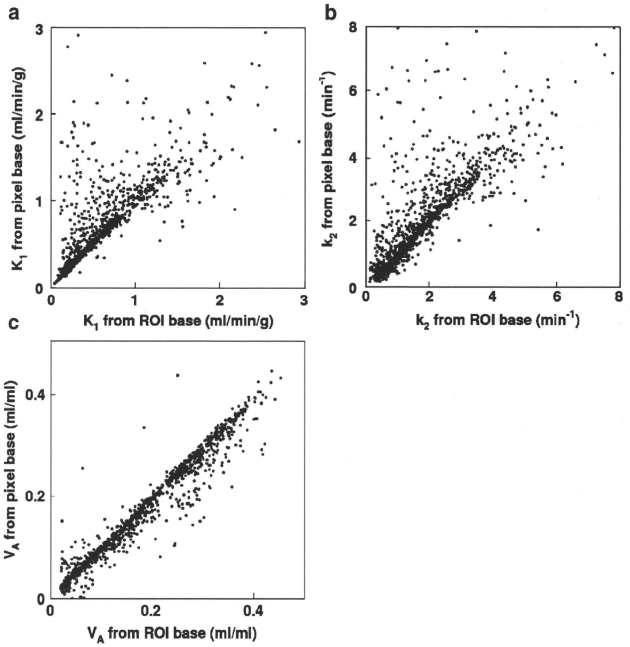

Fig. 2 Relationships of (**a**) K_1, (**b**) k_2 and (**c**) V_A between the ROI-based NLF method and pixel-based BFM. The regression lines were $K_{1,BFM}=0.93K_{1,NLF}-0.11$ ml/min/g ($r=0.80$, $p<0.001$), $k_{2,BFM}=0.96k_{2,NLF}-0.13$ ml/min/g ($r=0.77$, $p<0.001$), and $V_{A,BFM}=0.92V_{A,NLF}-0.00$ ml/ml ($r=0.97$, $p<0.001$)

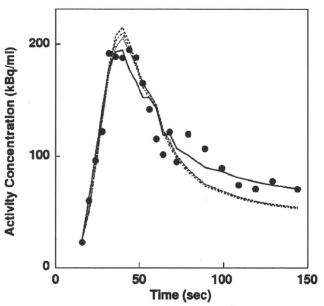

Fig. 3 Curves fitted to the measured tissue TAC from the different computation methods. Three parameters: K_1, k_2 and V_A were computed. p-fixed: K_1 and V_A were computed with p ($=K_1/k_2$) fixed at 0.35 ml/g. V_A-fixed: K_1 and k_2 were computed with V_A fixed at 0.15 ml/g. V_A-ignored: K_1 and k_2 were computed without taking into account V_A

parameter fitting fixing V_A in patient 2 and fixing p in patient 3, although some AIC values were similar (Table 2). These results show that the present method with three parameter fitting is feasible for computing RBF.

Values of K_1, $k_2 \cdot p_{phys}$ and V_A were obtained for the whole renal region and cortical region (Table 3). The K_1

Table 2 AIC values for the models

Subject	Three parameters[a]	p-fixed[b]	V_A-fixed (0.15)[c]	V_A-ignored[d]
1	484±20	519±28	499±15	494±15
2	474±9	486±14	474±9	477±8
3	525±12	523±8.3	527±10	527±7
4	483±14	497±21	501±12	506±13
5	497±18	502±19	508±32	499±13
6	496±11	507±14	500±9	497±9

[a] K_1 and k_2, V_A computed.
[b] K_1 and V_A computed with k_2 fixing such that $p=K_1/k_2=0.35$ ml/g.
[c] K_1 and k_2 computed with V_A fixed at 0.15 ml/g.
[d] K_1 and k_2 computed without taking into account V_A.

Table 3 Values of K_1, $k_2 \cdot p_{phys}$ and V_A (n=6) in the whole renal region and the cortical region calculated by the present method for the baseline conditions and the stimulated conditions

	K_1 (ml/min/g)	$k_2 \cdot p_{phys}$ (ml/min/g)	V_A (ml/ml)	GFR (ml/min/g)
Whole region				
Baseline	1.09±0.33	3.11±1.48	0.15±0.09	0.35±2[a]
Enalapril-stimulated	1.03±0.44	2.55±1.29	0.16±0.14	
Cortical region				
Baseline	1.57±0.60*	3.64±2.15*	0.18±0.12*	
Enalapril-stimulated	1.42±0.39*	3.55±1.64*	0.25±0.14*	

No significant difference was found between the baseline and stimulated conditions.
*Difference was significant between the whole and cortical regions.
[a] A kidney weight of 300 g and a cortex ratio of 70% were assumed.

values were smaller than $k_2 \cdot p_{phys}$ values and the ratio between them ranged from 0.35 to 0.45, suggesting that K_1 values underestimated RBF due to the partial volume effect. Both K_1 and $k_2 \cdot p_{phys}$ were not significantly different between the resting and stimulated conditions for the whole renal region and the cortical region, respectively, although the value of V_A was higher under the stimulated conditions than under the basal conditions. The GFR obtained was 78±4 ml/min, corresponding to a clearance rate of 0.37±0.02 ml/min/g and to 9.6% of the k_2 obtained for the cortical region under the normal conditions.

Representative K_1 and $k_2 \cdot p_{phys}$ images generated by the present method are shown in Fig. 4. The quality of the image is acceptable. The K_1 and $k_2 \cdot p_{phys}$ values ranged from 1.5 to 2.0 ml/min/g and 3.0 to 5.0 around cortical region, respectively, and some parts showed higher values than these. The average time required to compute the parametric images was 2 min 23 s.

Error analysis

The sizes of the errors introduced in both K_1 and k_2 were less than 20% for estimation of delay and the dispersion time constant up to 2 s (Fig. 5). The error sensitivity in K_1 and k_2 was 40% when the partition coefficient was 0.35 (Fig. 6). The magnitude of the error was markedly enhanced when the blood volume was ignored (Fig. 7a), and if the arterial blood volume increased by 25%, K_1 and k_2 were overestimated by 20% (Fig. 7a).

Discussion

We have presented an approach to generating quantitative K_1, k_2 and V_A images using $H_2{}^{15}O$ and PET applying the BFM computation method. The validity of this approach in healthy human subjects under resting and stimulated conditions is described. The rate constant values of K_1 and $k_2 \cdot p_{phys}$ obtained from the parametric images were consistent against NFL and the quality of the K_1 and $k_2 \cdot p_{phys}$ images obtained was acceptable. The smaller K_1 against $k_2 \cdot p_{phys}$ values suggested that the K_1 values underestimated the absolute RBF value due to the partial volume effect. The simulation showed that the delay time and dispersion time constant should be estimated within an accuracy of 2 s, and V_A and p cannot be ignored/fixed to

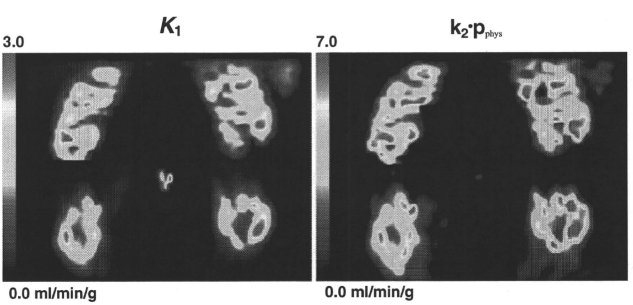

Fig. 4 Representative parametric images of K_1 (*left*) and $k_2 \cdot p_{phys}$ (*right*) for a subject under baseline conditions. Coronal (*upper*) and transverse (*lower*) views are shown

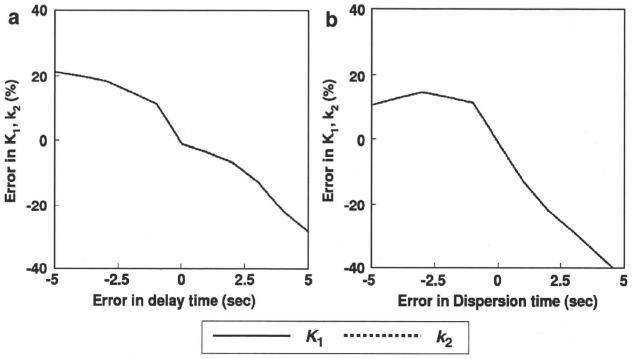

Fig. 5 Error propagation from the error in input time (**a**) and dispersion time constant (**b**) to K_1 and k_2 (the two lines were identical). Positive and negative values of error indicate over- and under-correction of delay time and dispersion time, respectively

estimate the rate constants of K_1 and/or k_2. Also V_A cannot be ignored, even when only relative rate constant values are needed. These findings suggest that the present k_2 obtained BFM technique provides an RBF image with reasonable accuracy and quality.

In the present study the rate constants of K_1 and k_2 were experimentally computed, and the ratios obtained ranged from 0.35 to 0.45 ml/g, which corresponds to the apparent kidney–blood partition coefficient. The much smaller apparent p value might be due to a partial volume effect, as has been demonstrated in a previous brain and cardiac study [10, 11], because of the composite structure of the kidney, the spatial resolution of the reconstructed image and breathing movement of the patient during the scan. When the rate constant K_1 is underestimated due to the partial volume effect, $k_2 \cdot p_{phys}$ could be applied for RBF rather than K_1. The present study showed that the contribution of GFR to the clearance rate was only 10%, and that $k_2 \cdot p_{phys}$ is more appropriate for RBF assessment, although further study of how the GFR changes under stimulated conditions is required. The $k_2 \cdot p_{phys}$ value in the cortical region obtained in the present study was 3.64±2.15 ml/min/g under normal condition, a value within the normal range of 4 to 5 ml/min/g reported in the literature [22]. Middlekauff et al. [23–25] applied the ROI base analysis, and showed similar RBF values around 4 ml/min/g. These findings also support the use of $k_2 \cdot p_{phys}$ for the calculation of RBF. The different values of RBF between the present study and the previous studies [3–5] might be due to differences in the approaches.

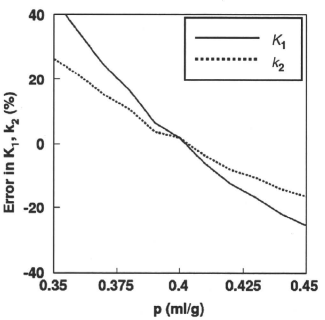

Fig. 6 Error propagation from the partition coefficient (p, ml/g) to K_1 and k_2. When the true p was varied between 0.6 and 0.8 ml/g, the size of the error in RBF was simulated assuming p=0.7 ml/g

The present computation of RBF by the BFM has two main advantages over the NLF. One is the ability to produce a voxel-by-voxel quantitative parametric map, and the other is faster computing speed. In fact, the parametric images were obtained within a reasonable time, i.e. 2.5 min with an image size of 128×128 pixels with 35 slices and 22 frames. The time could be further reduced by applying a threshold to omit pixels with lower values. From a clinical standpoint, voxel-by-voxel analysis is preferred to ROI-based analysis because the operator can independently define ROIs to improve reproducibility, and faster computations are important for analysing very large datasets.

Kinetic parameters estimated by the NLF agreed well with those estimated by the BFM as shown in Fig. 2. The disagreement in some rate constant values between the voxel-based (BFM) and ROI-based computation methods might have been due to the composite structure between the cortical region and its surroundings, or to image noise. Although superior to the NLF in terms of computing speed and ability to generate parametric maps, the BFM shares the same source of errors as the NLF because they use the

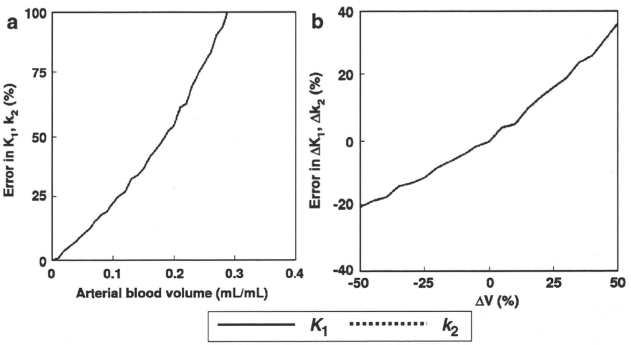

Fig. 7 **a** Error propagation from the arterial blood volume (V_A, ml/ml) to K_1 and k_2 (the two lines were identical). When the true V_A changed from 0.0 to 0.4 ml/ml, the size of the error in K_1 and k_2 calculated assuming V_A=0.0 ml/ml was simulated. **b** Error propagation from the change in arterial blood volume from 0.14 ml/ml (ΔV_A) to the change in K_1 and k_2 from the initial conditions (ΔK_1 and Δk_2, ml/min/g) (the two lines were identical)

same model and assumption. Delay and dispersion in input function, motion of the patient during a study [26–28], and flow heterogeneity [29] are sources of error for parameters estimated by both the NLF and BFM. Selection of a specific range of k_2 and the number of basis function can affect the accuracy and precision of the estimated parameters in neuroreceptor studies [30, 31]. However, the range was 0 to 15 ml/min/g in the present computation with $H_2{}^{15}O$, and the limits of this range would be acceptable for the present computation. In practice, selection of a wider range and/or a large number of discrete values of the basis function is slow and inefficient against the required accuracy and precision.

The present simulation study showed that if V_A is neglected or fixed, not only the absolute rate constants, i. e. RBF value, are overestimated, but estimated changes in RBF between two physiological states could be over- or underestimated. These findings suggest that V_A should be included to obtain either absolute or relative values of RBF. For p, the present simulation revealed that the error sensitivity in RBF for that value was significant. The values of p for the whole and cortical regions were 0.35 and 0.42 ml/g, respectively. If the value was fixed at 0.4 ml/g, a 40% overestimation in RBF for regions with a p of 0.35 occurred. Thus, regional difference in p introduce error in quantitative RBF values. Also the AIC analysis showed that introducing the extra parameters of p and V_A did not increase the AIC value against the others. These findings suggest that both p and V_A need to be estimated simultaneously with quantitative RBF, especially when changes under different conditions are assessed.

Knowledge of RBF is mostly needed in determining the severity of renovascular disease. Although the degree of renal artery stenosis is easily diagnosed, its actual effect on RBF remains difficult to quantify. In clinical work, estimates of GFR have not shown very good accuracy in relation to possible interventional treatment. Also, there is no good clinical method to easily measure single-kidney or regional RBF. We can obtain the effective renal plasma flow (ERPF) by infusing *p*-aminohippuric acid and measuring the urine and plasma concentrations, but this method only gives the total ERPF for both kidneys. An alternative is a magnetic resonance (MR) based method, which is problematic in patients with chronic kidney disease, because the contrast agent gadolinium is contraindicated in these subjects [32]. The present PET-related methodology may provide quantitative estimate of regional RBF, and be clinically applicable under conditions such as chronic allograft nephropathy and acute kidney insufficiency. The procedure – as presented here – still involves a small degree of invasiveness because of blood sampling. However, many noninvasive methods for estimating input functions have been proposed [3–5, 23–25, 33, 34], and their implementation will allow RBF to be determined in a fully noninvasive fashion, particularly for clinical purposes.

In conclusion, although some issues remain to be investigated, this study shows the feasibility of measurement of RBF using PET with $H_2{}^{15}O$.

Acknowledgments The authors thank the technical staff of the Turku PET Centre for their effort and skill dedicated to this project. This work was supported by the Hospital District of Southwest of Finland and was conducted within the "Centre of Excellence in Molecular Imaging in Cardiovascular and Metabolic Research" supported by the Academy of Finland, University of Turku, Turku University Hospital and Abo Academy. The study was further supported by grants from the Academy of Finland (206359 to P.N.), the Finnish Diabetes Foundation (P.I.), EFSD/Eli-Lilly (P.I.), the Sigrid Juselius Foundation (N.K. and P.I.), and the Novo Nordisk Foundation (P.N.).

References

1. Nitzsche EU, Choi Y, Killion D, Hoh CK, Hawkins RA, Rosenthal JT, et al. Quantification and parametric imaging of renal cortical blood flow in vivo based on Patlak graphical analysis. Kidney Int 1993;44:985–96.
2. Szabo Z, Xia J, Mathews WB, Brown PR. Future direction of renal positron emission tomography. Semin Nucl Med 2006;36:36–50.
3. Juillard L, Janier MF, Foucue D, Lionnet M, Le Bars D, Cinotti L, et al. Renal blood flow measurement by positron emission tomography using 15O-labeled water. Kidney Int 2000;57:2511–18.
4. Juillard L, Janier MF, Fouque D, Cinotti L, Maakel N, Le Bars D, et al. Dynamic renal blood flow measurement by positron emission tomography in patients with CRF. Am J Kidney Dis 2002;40:947–54.
5. Alpert NM, Rabito CA, Correia DJA, Babich JW, Littman BH, Tompkins RG, et al. Mapping of local renal blood flow with PET and H215O. J Nucl Med 2002;43:470–75.
6. Anderson HL, Yap JT, Miller MP, Robbins A, Jones T, Price PM. Assessment of pharmacodynamic vascular response in a phase I trial of combretastatin A4 phosphate. J Clin Oncol 2003;21:2823–30.
7. Anderson H, Yap JT, Wells P, Miller MP, Propper D, Price D, et al. Measurement of renal tumour and normal tissue perfusion using positron emission tomography in a phase II clinical trial of razoxane. Br J Cancer 2003;89:262–67.
8. Snyder WS, Cook MJ, Nasset ES, Karhausen LR, Howells GP, Tipton IH. Report of the Task Group on Reference Man. London: Pergamon Press; 1974. p. 175–77.
9. Herscovitch P, Raichle ME. What is the correct value for the brain–blood partition coefficient for water? J Cereb Blood Flow Metab 1985;5:65–9.
10. Iida H, Law I, Pakkenberg B, Krarup-Hansen A, Eberl S, Holm S, et al. Quantitation of regional cerebral blood flow corrected for partial volume effect using O-15 water and PET: I. Theory, error analysis, and stereologic comparison. J Cereb Blood Flow Metab 2000;20:1237–51.
11. Blomqvist G, Lammertsma AA, Mazoyer B, Wienhard K. Effect of tissue heterogeneity on quantification in positron emission tomography. Eur J Nucl Med 1995;22:652–63.
12. Koeppe RA, Holden JE, Ip WR. Performance comparison of parameter estimation techniques for the quantitation of local cerebral blood flow by dynamic positron computed tomography. J Cereb Blood Flow Metab 1985;5:224–34.
13. Gunn RN, Lammertsma AA, Hume SP, Cunningham VJ. Parametric imaging of ligand-receptor binding in PET using a simplified reference region model. Neuroimage 1997;6:279–87.
14. Watabe H, Jino H, Kawachi N, Teramoto N, Hayashi T, Ohta Y, et al. Parametric imaging of myocardial blood flow with 15O-water and PET using the basis function method. J Nucl Med 2005;46:1219–24.
15. Boellaard R, Knaapen P, Rijbroek A, Luurtsema GJ, Lammertsma AA. Evaluation of basis function and linear least squares methods for generating parametric blood flow images using 15O-water and positron emission tomography. Mol Imaging Biol 2005;7:273–85.
16. Ruotsalainen U, Raitakari M, Nuutila P, Oikonen V, Sipilä H, Teräs M, et al. Quantitative blood flow measurement of skeletal muscle using oxygen-15-water and PET. J Nucl Med 1997;38:314–19.
17. Levey A, Bosch J, Lewis J, Greene T, Rogers N, Roth D. A more accurate method to estimate glomerular filtration rate from serum creatinine: a new prediction equation. Modification of Diet in Renal Disease Study Group. Ann Intern Med 1999;130:461–70.
18. Iida H, Kanno I, Miura S, Murakami M, Takahashi K, Uemura K. Error analysis of a quantitative cerebral blood flow measurement using H215O autoradiography and positron emission tomography, with respect to the dispersion of the input function. J Cereb Blood Flow Metab 1986;6:536–45.
19. Iida H, Higano S, Tomura N, Shishido F, Kanno I, Miura S, et al. Evaluation of regional differences of tracer appearance time in cerebral tissues using [15O] water and dynamic positron emission tomography. J Cereb Blood Flow Metab 1988;8:285–88.
20. Akaike H. A new look at the statistical model identification. IEEE Trans Automat Contr 1974;AC19:716–23.
21. Kudomi N, Hayashi T, Teramoto N, Watabe H, Kawachi N, Ohta Y, et al. Rapid quantitative measurement of CMRO2 and CBF by dual administration of 15O-labeled oxygen and water during a single PET scan – a validation study and error analysis in anesthetized monkeys. J Cereb Blood Flow Metab 2005;259:1209–24.
22. Ganong WF. Review of medical physiology. 8th ed. Norwalk: Appleton & Lange; 1977. p. 522–45.
23. Middlekauff HR, Nitzsche EU, Hamilton MA, Schelbert HR, Fonarow GC, Moriguchi JD, et al. Evidence for preserved cardiopulmonary baroflex control of renal cortical blood flow in humans with advanced heart failure. Circulation 1995;92:395–401.
24. Middlekauff HR, Nitzsche EU, Hoh CK, Hamilton MA, Fonarow GC, Hage A, et al. Exaggerated renal vasoconstriction during exercise in heart failure patients. Circulation 2000;101:784–89.
25. Middlekauff HR, Nitzsche EU, Hoh CK, Hamilton MA, Fonarow GC, Hage A, et al. Exaggerated muscle mechanoreflex control of reflex renal vasoconstriction in heart failure. J Appl Physiol 2001;90:1714–19.
26. Fulton RR, Meikle SR, Eberl S, Pfeiffer J, Constable CJ. Correction for head movements in positron emission tomography using an optical motion-tracking system. IEEE Trans Nucl Sci 2002;49:116–23.
27. Bloomfield PM, Spinks TJ, Reed J, Schnorr L, Westrip AM, Livieratos L, et al. The design and implementation of a motion correction scheme for neurological PET. Phys Med Biol 2003;48:959–78.
28. Woo SK, Watabe H, Choi Y, Kim KM, Park CC, Iida H. Sinogram-based motion correction of PET images using optical motion tracking system and list-mode data acquisition. IEEE Trans Nucl Sci 2004;51:782–88.
29. Herrero P, Staudenherz A, Walsh JF, Gropler RJ, Bergmann SR. Heterogeneity of myocardial perfusion provides the physiological basis of perfusable tissue index. J Nucl Med 1995;36:320–27.
30. Cselényi Z, Olsson H, Halldin C, Gulyás B, Farde L. A comparison of recent parametric neuroreceptor mapping approaches based on measurements with the high affinity PET radioligands [11C]FLB 457 and [11C]WAY 100635. Neuroimage 2006;32:1690–708.
31. Schuitemaker A, van Berckel BN, Kropholler MA, Kloet RW, Jonker C, Scheltens P, et al. Evaluation of methods for generating parametric (R-[11C]PK11195 binding images. J Cereb Blood Flow Metab 2007;27:1603–15.
32. Martin D, Sharma P, Salman K, Jones RA, Grattan-Smith JD, Mao H, et al. Individual kidney blood flow measured with contrast-enhanced first-pass perfusion MR imaging. Radiology 2008;246:241–48.
33. Iida H, Kanno I, Takahashi A, Miura S, Murakami M, Takahashi K, et al. Measurement of absolute myocardial blood flow with H215O and dynamic positron-emission tomography strategy for quantification in relation to the partial-volume effect. Circulation 1988;78:104–15.
34. Germano G, Chen BC, Huang S-C, Gambhir SS, Hoffman EJ, Phelps ME. Use of the abdominal aorta for arterial input function determination in the hepatic and renal PET studies. J Nucl Med 1992;33:613–20.

A method to measure PET scatter fractions for daily quality control

H. W. de Jong[a)]
Department of Radiology and Nuclear Medicine, University Medical Centre, P. O. Box 85500, 3508 GA, Utrecht, The Netherlands and Department of Nuclear Medicine and PET Research, VU University Medical Centre, P. O. Box 7057, 1007 MB, Amsterdam, The Netherlands

M. Lubberink
Department of Nuclear Medicine and PET Research, VU University Medical Centre, P. O. Box 7057, 1007 MB, Amsterdam, The Netherlands

H. Watabe and H. Iida
Department of Investigative Radiology, National Cardiovascular Center Research Institute, 5-7-1 Fujishirodai, Suita, Osaka 565-8565, Japan

A. A. Lammertsma
Department of Nuclear Medicine and PET Research, VU University Medical Centre, P. O. Box 7057, 1007 MB, Amsterdam, The Netherlands

(Received 25 March 2009; revised 27 July 2009; accepted for publication 29 July 2009; published 14 September 2009)

Purpose: Regular monitoring of PET scanner performance is mandatory to assure quality of acquired data. While extensive performance measurements include many scanner characteristics such as resolution, count rate, uniformity, sensitivity, and scatter fraction (SF), most daily QC protocols are limited to uniformity and sensitivity measurements. These measurements may be too insensitive to detect more subtle drifts in detector gains that could lead to reduced detection of primary and increased detection of scattered events. Current methods to measure SF, such as those prescribed by the NEMA protocols (SF-NEMA), however, require specially designed phantoms and are too cumbersome to be performed on a daily basis.

Methods: In this study, a simple and versatile method to determine SF is described. This method (SF-DAILY) does not require additional measurements, making it suitable for daily QC. The method was validated for four different scanners by comparing results with those obtained with the NEMA 1994 protocol.

Results: For all scanner types and acquisition modes, excellent agreement was found between SF-NEMA and SF-DAILY.

Conclusions: The proposed method is a very practical and valuable addition to current daily QC protocols. In addition, the method can be used to accurately measure SF in phantoms with other dimensions than the NEMA phantom. © *2009 American Association of Physicists in Medicine.* [DOI: 10.1118/1.3213096]

Key words: PET, scatter fraction, quality control, NEMA

I. INTRODUCTION

Assessment of PET scanner performance is mandatory to prevent image artifacts and to assure quantitative integrity of acquired data. In general, extensive performance measurements are performed only occasionally, e.g., after scanner installation, an upgrade, or major maintenance, with more concise quality control (QC) measurements being performed on a daily basis (daily QC). The purpose of this daily QC is to detect scanner malfunctioning and to monitor scanner stability. Ideally, this daily QC should be sensitive enough to detect changes in scanner performance that require (immediate) attention. As scanner maintenance may have substantial impact on patient throughput and planning, however, a decision to perform maintenance should be well founded, preferably based on a more extensive set of measured parameters. Therefore, it is important that daily QC tests provide as much relevant information as possible. Apart from offering a solid basis for decision making in clinical practice, daily QC data can also give insight in scanner behavior as a function of temperature, power loss, or time after maintenance.

While the above mentioned extensive (acceptance) performance measurements (using a range of different phantoms) include many scanner characteristics such as uniformity, sensitivity, and scatter fraction (SF), for practical reasons, the daily QC often is restricted to detector uniformity and sensitivity. These parameters are typically derived from a scan of a uniform cylindrical phantom filled with the long-lived isotope ^{68}Ge. These limited measurements may, however, obscure scanner drift or inaccuracies caused by changing detector gains, possibly leading to reduced detection of primary and increased detection of scattered events. In addition, drifts in electronics settings can lead to loss of sensitivity. For example, a shift in photomultiplier tube (PMT) gains can cause the 511 keV photopeak to drift, eventually (partly) falling outside the energy window.[1] This, in turn, may lead to a direct change in the detected SF, and hence image quality

and quantitative accuracy. Especially in state-of-the-art PET scanners that can only operate in 3D mode, SF is high (typically 50% of all detected events) and alterations in measured SF can have a major impact. In order to quantify 3D PET data, sophisticated scatter correction algorithms have been developed. If adjustments are not made while needed, however, changes in SF can cause the algorithm to over- or underestimate the scatter contribution, leading to bias, i.e., incorrect regional activity concentrations.

The SF is defined as the fraction of all events that have been scattered prior to detection. There are many ways to determine this SF, but the most widely accepted method is according to the NEMA standards. NEMA protocols have been established in a collaboration between scanner manufacturers and users. The advantage of NEMA protocols is that results can be interpreted by all parties, without uncertainties about the exact conditions under which measurements were performed. This is especially useful when communicating results between users, manufacturers, or other parties. Disadvantages of NEMA protocols are that they usually require specially designed setups and phantoms and that they are too cumbersome for use on a daily basis. Consequently, NEMA protocols often are used only for acceptance testing and in other situations where extensive measurements are required (e.g., following a major upgrade).

The purpose of the present study was to develop and validate a simple method to accurately estimate scatter fractions using a uniform cylindrical phantom. In general, a uniform cylindrical phantom is used to monitor sensitivity and uniformity on a daily basis and, therefore, this SF method could easily be added to the daily or weekly QC without the need for additional measurements. Validation was performed by comparing measured SF values with those derived according to the NEMA NU-1994 protocol using four different scanners.

II. MATERIALS AND METHODS

II.A. NEMA scatter fraction

NEMA standards for PET instrumentation describe a series of phantom measurements to determine scanner characteristics, including spatial resolution, scatter fraction, count rates, sensitivity, accuracy of correction methods, and general image quality. While the older NEMA-1994 protocol[1,2] was defined in a time when PET was primarily used as a brain imaging modality, the 2001 and 2007 protocols reflect the shift toward whole-body oncological applications.[3–6] For the SF measurement this is illustrated by the short 20 cm cylinder in the NEMA 1994 protocol (SF-NEMA1994) and the longer 70 cm cylinder in the NEMA 2001 protocol (SF-NEMA2001). The latter phantom was introduced to include scatter that originates from outside the axial field of view (FOV) of the scanner, and therefore SF-NEMA2001 is higher than SF-NEMA1994, especially when scanning in 3D mode (i.e., without septa in the FOV). In a comparative study, however, it was shown that a change in SF-NEMA1994 strongly correlated with a change in SF-NEMA2001.[3]

As the cylindrical daily QC phantom often has the same dimensions as the NEMA1994 scatter fraction phantom, SF-NEMA1994 was used as the gold standard for validating the proposed method. The NEMA1994 protocol describes a 20 cm diameter, 20 cm length, water filled cylinder in which a 20 cm line source can be inserted at three different positions (0, 45, and 90 mm from the center) (Fig. 1). After filling the line source with a low level of activity (~5 kBq/cc of ^{18}F), it was inserted at each of the three positions and, at each position, data were acquired for 15 min to ensure at least 200 kcounts per slice within the central 17 cm of the phantom.

SF-NEMA1994 was then obtained by (1) correcting the three measurements for ^{18}F decay, detector nonuniformities (normalization), and, where relevant, detector gaps (Fig. 1), (2) straightening the sinograms to eliminate curves due to off-center line source positions (Fig. 1), (3) setting all sinogram pixels corresponding to positions >12 cm from the center of the phantom to zero, (4) adding projection angles to create one profile per line source position, and (5) adding the three scatter profiles, thereby weighting for the annular region in which the line source is positioned, where (6) scattered events under the primary peaks were estimated using linear interpolation between count levels within 2 cm from the peak[2] (Fig. 1).

II.B. Simplified procedure

When acquiring PET data using a uniform cylindrical phantom of diameter D, filled with an arbitrary activity and placed centrally in the FOV, the resulting total count (T) projections are the sum of primary (or unscattered) events (P), scattered events (S), and random events. In general, randoms are corrected for by subtracting an independently measured estimate, usually obtained with the delayed window technique and therefore not addressed specifically in this study.[7] If r is the position on the projection (bin position) relative to the center of the FOV, then $S(r)$ is an arbitrary function describing the scatter background. The point spread function PSF(r) is a 1D function describing the resolution of the projection data centered around $r=0$ (Fig. 2). It is now postulated that, for a nonoblique projection plane, the spatial distribution of the total counts T of primary and scattered events within the FOV of a single ring of detectors (or nonoblique, direct plane) originating from a cylindrical phantom with diameter D is given by

$$T(r) = \mathrm{PSF}(r) \otimes (P(r,D,p) + S(r)),$$

$$P(r,D,p) = 2\sqrt{\frac{1}{4}D^2 - r^2}\cdot p \cdot \exp\left(-\mu\sqrt{\frac{1}{4}D^2 - r^2}\right), \quad r \le D,$$

$$P(r,D,p) = 0, \quad r > D, \tag{1}$$

where μ is the linear attenuation coefficient at 511 keV (cm^{-1}), $P(r,D,p)$ describes the distribution of the detected primary photons, and p is a scaling factor for the total number of detected primary photons that depends on both activity

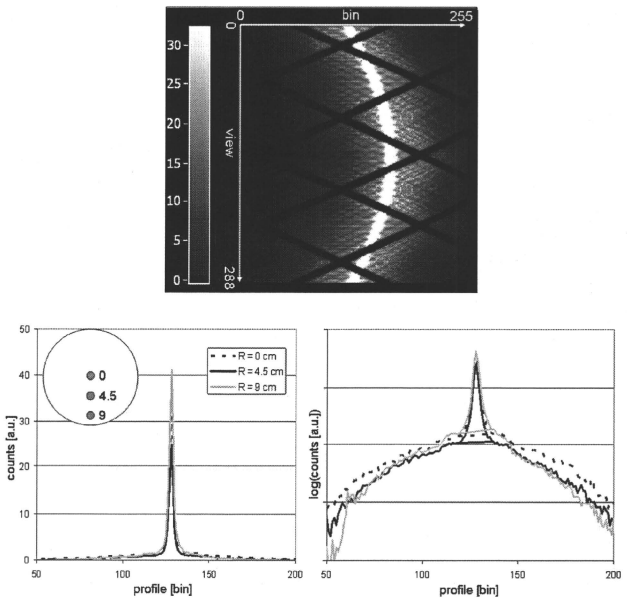

FIG. 1. Illustration of SF-NEMA procedure. The top image shows a sinogram from a line measurement for one of the three positions. Line profiles (bottom) are generated by straightening the profiles and averaging all views of the sinogram. Profiles are also shown using a logarithmic scale including the interpolated curves between ±2 cm (this case ±16 bins) from the center for scatter estimation. Using these curves primary and scatter fractions are extracted by integrating the profiles as described by the NEMA protocol.

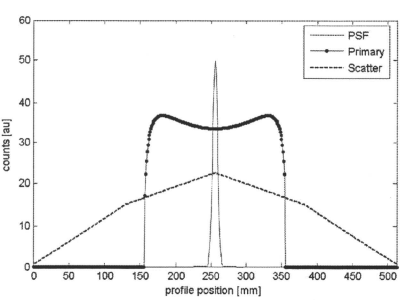

FIG. 2. Example of the three parts of the model used for estimating the SF-Daily: A PSF with a FWHM of 7 mm (scaled for illustration purposes), a primary response from a cylinder with a diameter of 20 cm, and an arbitrary scatter response.

in the phantom and sensitivity of the scanner. In short, the total response is a sum of primary and scatter events, where the shape of the primary contribution is known. In this case the activity of the nonoblique cross section through the cylindrical phantom was approximated by a circle [first term of $P(r,D,p)$], and multiplication with the attenuation factor (last exponential term) estimates the shape of the response in the absence of scattered photons.

In this study $S(r)$ was modeled as a first order cubic spline[8] based on a set of control points $(r_1,y_1;\ldots;r_n,y_n)$, i.e., $S(r)$ was simply modeled as a piecewise linear function between the coordinates (r_1,y_1) and (r_2,y_2), (r_2,y_2) and (r_3,y_3), and so on. Although a piecewise linear shape might not be natural, the convolution with PSF(r) removes discontinuities at the control points. Figure 2 gives an example of the components $P(r)$, $S(r)$, and PSF(r).

The new simplified method to derive SF (SF-Daily) makes direct use of Eq. (1). First, the PSF is modeled using a Gaussian function with a fixed width based on scanner specific resolution data. For the sake of simplicity, in all cases a spatially invariant resolution was assumed. Next, for the scatter function $S(r)$, the control points are chosen

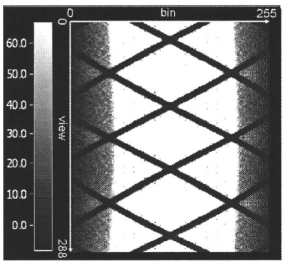

FIG. 3. Sinogram of uniform cylinder used for daily QC measurements. Scatter in the background of the sinogram is clearly visible. Black diagonal lines are due to gaps between detectors heads

equally divided over the data space (r direction) with r_1 located at the beginning and r_n at the end of the transversal field of view. For this study five control points were used. Since D, μ, and PSF(r) are known and $r_1,\ldots,r_5$ are fixed, $T(r)$ has p and the five base points $y_1,\ldots,y_5$ as free parameters. These parameters were estimated by fitting $T(r)$ to a measured response projection profile using a nonlinear curve fitting method (Levenberg-Marquardt[9]). It should be emphasized here that Eq. (1) is fitted to all projection data and not just to the tails of the sinogram, making the method very robust. For calculating SF only counts in the region $r \pm 3/5D$ are taken into account as this is prescribed by the NEMA protocol:

$$\mathrm{SF} = \frac{\int_{-3/5D}^{3/5D} S(r)dr}{\int_{-3/5D}^{3/5D} T(r)dr}. \tag{2}$$

To acquire data, a uniformly filled cylindrical phantom with known diameter (in the present case 20 cm for the whole-body scanners and 4.5 cm for the animal scanner) has to be placed in the center of the FOV, with its long axis in line with the scanner axis. In case the scanner has scintillation crystals containing intrinsic radioactivity such as L(Y)SO, background radiation has to be taken into account, as it produces randoms and a small fraction of true coincidences due to cascading gamma rays.[10] This background activity, however, usually is very low (typically less than 1×10^{-5} counts per second per line of response). On the other hand care should be taken not to induce pileup effects that can alter SF due to high count rates. Although this differs from scanner to scanner, as an example, SF for the high resolution research tomography (HRRT) is stable when total activity in the FOV is between approximately 1 and 100 MBq.[11] Although the count rate has negligible effect on SF as long as it is kept within the clinical range, ideally, total activity in the cylinder should be comparable to that used for the NEMA protocol (2.5 kBq cc^{-1}, or 15 MBq). Figure 3 shows an example of an acquired sinogram.

II.C. Scanners

To test and validate the new SF-Daily method under various circumstances, data from four different PET scanners were used. The scanners varied in crystal material, crystal size, ring diameter, and axial field of view, characteristics that all affect the scatter fraction. Table I gives an overview of relevant scanner data.

The Siemens HR (also known as ECAT Exact 47)[12] is a whole-body BGO scanner that can be operated in both 2D and 3D modes by means of retractable septa. Although 3D acquisitions yield higher sensitivity, the 2D mode is characterized by smaller randoms and scatter fractions, which can be advantageous for high count rate studies. The Philips Allegro[13] is a 3D only whole-body scanner based on curved GSO crystals, which have the advantage of a relatively high energy resolution compared with other PET crystals, resulting in a lower SF. The 3D only Siemens HRRT was one of the first scanners to apply LSO crystals. Its high spatial resolution enables detailed brain studies and small animal applications that can be covered in one bed position, thanks to the large axial FOV.[11] The Siemens microPET Focus 120 (Ref. 14) is a dedicated small animal LSO scanner with a gantry opening of approximately 20 cm. Although a new NEMA protocol specifically for small animal PET scanners was introduced only recently[15] microPET experiments using NEMA-like phantoms have already been reported previously.[16] Table I also lists resolution data (mm FWHM) as used for modeling PSF in Eq. (1).

II.D. Scatter fraction measurements

SF-NEMA and SF-Daily were measured and compared for all four scanners. For the HR, SF was measured using a cylinder, filled with ^{18}F, in both 2D and 3D acquisition modes. This provided a means to evaluate the effects of septa on measured SF for both methods. Although in most cases 3D sinograms were acquired, analysis was performed only on nonoblique (direct) planes in the sinogram. Hence, all

TABLE I. Relevant data of the various scanners.

Scanner	Crystal material	Crystal thickness (mm)	Axial FOV (cm)	Diameter gantry (cm)	Resolution used (mm FWHM)	Ring diameter (cm)
Siemens HR	BGO	30	15	51	5	82.7
Philips Allegro	GSO	20	18	56	5	86.4
Siemens HRRT	LSO	20	25	31	3	46.9
Siemens microPET Focus 120	LSO	10	7.6	20	2	25.8

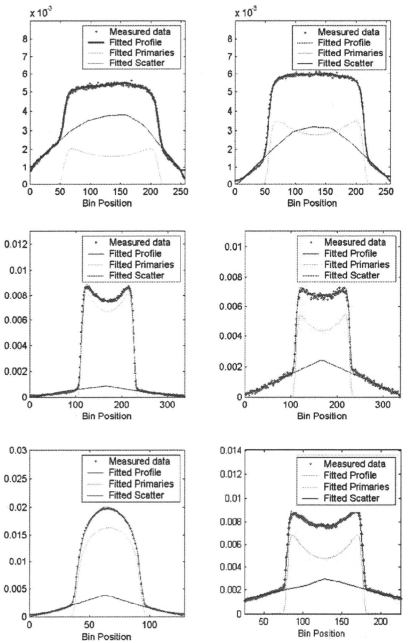

FIG. 4. Profiles of measured and fitted data. Top: HRRT before (left) and after (right) scanner setup. Mid: HR in 2D (left) and 3D (right) acquisition mode. Bottom: MicroPET (left) and Allegro (right). Due to the normalization process vertical units are arbitrary.

oblique planes (also called segment 1 and higher) were disregarded, effectively resulting in a 2D sinogram.

For the HRRT, SF-Daily was measured using a ^{68}Ge phantom (diameter of 20 cm, length of 27 cm, 20 MBq), routinely used for daily QC purposes. Sensitivity of SF-NEMA to small changes in SF was investigated by measuring SF of the HRRT just before and after performing a setup process (i.e., tuning of gain and other settings in order to maximize performance), as this setup process will decrease SF due to optimized energy calibration. SF was measured for the whole gantry and plane by plane. To assess effects of noise, SF-Daily for the whole gantry was measured using acquisition times of 15, 2, and 1 min.

For the Allegro, SF was determined for different lower energy threshold settings (260, 310, 360, and 410 keV) and an upper level discriminator set to 665 keV in order to investigate the correlation between both SF methods. For this a 20 cm diameter, 20 cm length cylinder filled with 20 MBq ^{18}F was used. As no mini-scatter-phantom was available for the microPET Focus 120, only SF-Daily was measured using a cylinder with an inner radius of 4.5 cm and a length of 10 cm, filled with 10 MBq, and this measurement was compared with published SF-NEMA values.[4]

TABLE II. Comparison of SF-NEMA and SF-Daily.

Scanner	SF-NEMA (%)	SF-Daily (%)
HRRT before setup	63	63
HRRT after setup	50	51
HRRT 15 min	50	51
HRRT 2 min	50	50
HRRT 1 min	50	50
HR 2D	14	13
HR 3D	38	33
MicroPET 45mm diameter cylinder	27[a]	23
Allegro	36	34

[a]The SF-NEMA was determined for a 60 mm phantom (8).

III. RESULTS

Sinogram profiles of the central axial plane and SF-Daily curve fits of total response $T(r)$ according to Eq. (1) are shown in Fig. 4 for all scanners. In addition, resulting primary $P(r)$ and scattered events $S(r)$ are shown. In all cases, the analytical response function equation (1) could be fitted to the data with high accuracy. Clearly, both shape and amplitude of the scatter distribution differ among scanners and acquisition modes. The HRRT setup process resulted in a lower SF and a more symmetric scatter distribution. Differences in scatter contribution between 2D and 3D modes are clearly illustrated by the HR profiles. The HR in 3D mode and the Allegro (measured using the lower level discriminator set at 410 keV) have similar profiles, indicating the impact of scanner geometry. The shape of the fitted primaries of the microPET deviates substantially from that of the other scanners due to the much smaller size of the phantom used. In general, SF measurement using SF-Daily were relatively insensitive to changes in PSF. Typically, doubling PSF (e.g., from 5 to 10 mm) resulted in only a 10% change in SF-Daily.

Table II summarizes SF values as obtained with SF-Daily and SF-NEMA. In addition, in case of the HRRT, SF values for different noise levels are included. Plane-by-plane SF values for the HRRT are shown in Fig. 5.

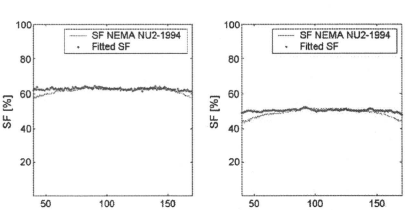

FIG. 5. Plane-by-plane values of SF-NEMA and SF-Daily (fitted SF) for the HRRT before (left) and after (right) setup.

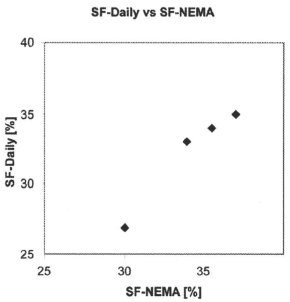

FIG. 6. SF-Daily and SF-NEMA values measured on the Allegro. Data points with higher SF refer to measurements with lower threshold values (260, 310, 360, and 410 keV).

Figure 6 shows SF values of the Philips Allegro for varying lower energy threshold settings. Both SF-NEMA and SF-Daily increased slightly with decreasing threshold channel, and a good correlation between both methods was found (R^2=0.96). Finally, Fig. 7 shows a Bland-Altman plot of the combined results presented in Table II and Fig. 6.

IV. DISCUSSION AND CONCLUSION

Using a simple curve fitting method, SF-Daily values were determined for different scanners and acquisition modes and compared to SF-NEMA values. A difference between SF-Daily and SF-NEMA only existed for the HR in 3D mode and for the microPET. For the latter, however, SF-Daily was measured using a cylinder with an inner diameter of 4.5 cm, while published SF-NEMA data were obtained with a cylinder of 6 cm diameter. The impact of noise was negligible for the three acquisition times investigated. The count rate in the HRRT scans was approximately 50 kcounts per slice, resulting in more than 100 counts per bin in the 1 min profiles, apparently sufficient for an accurate fit. The

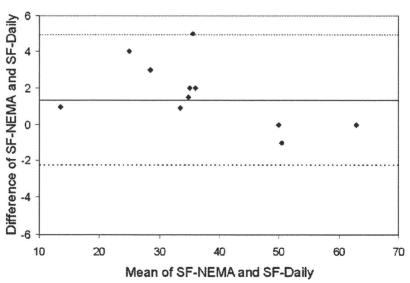

FIG. 7. Blant-Altman plot of all SF data from all four scanners and scan modes (data from Table II).

plane-by-plane comparison of SF-Daily and SF-NEMA showed good agreement especially in the center of the FOV. The slight deviation for the outer planes is probably due to the slightly longer phantom used for SF-NEMA than for SF-Daily.

In general, slight deviations in fitted and acquired profiles could be seen, especially at the maxima of the response (Fig. 4). Most likely these deviations are due to the fact that the thickness of the wall of the cylinder was not taken into account. Nevertheless, they have negligible effect on the resulting SF.

Similar to SF-NEMA, SF-Daily can be performed on either only a subset of the total sinogram, e.g., only on nonoblique (direct) planes, or on all sinogram planes/segments via a rebinning step.[5] The latter requires slight adaption of Eq. (1), as the primary response in oblique planes will be based on an oblique cross section of the phantom (in case of a cylinder this will become an ellipse) rather than a circle. In this study SF values were only determined using direct (2D) sinograms for both the SF-NEMA and SF-Daily methods. For one scanner these sinograms were derived from data acquired in both 2D mode (with septa) and 3D mode (without septa) in order to test different levels of scatter and randoms.

Although the SF-Daily method does require that the phantom is positioned in the center of the FOV, in practice it proved to be insensitive to slight misplacements. The method could, however, easily be extended with an algorithm to align the sinogram, similar to the SF-NEMA requirement.

One limitation is that not all scanners use cylindrical phantoms for daily QC purposes but rely on measurements of small sources in air. Although this has the benefit of requiring less activity, it gives the energy resolution at 511 keV rather than the scatter fraction. Furthermore, use of a point source in air also prohibits measurement of uniformity of coincidence timing over a large area of the FOV.

It should be emphasized that SF-Daily fits a profile to all projection data. This is in contrast to some scatter correction methods[17] that rely on fitting the tails of the scatter profile. In the presented approach all data are used and that knowledge about the primary response is included, making the method robust and insensitive to noise.

In general, SF-Daily values obtained were in close agreement with those derived using the NEMA protocol, making the method sufficiently sensitive to detect small changes in SF. Because the shape of the primary distribution is well known, accurate fits of the sum of scatter and primary events to the total profile can be achieved, without making prior assumptions about the shape of the scatter distribution. Furthermore no discontinuities in the estimated responses $S(r)$ were found. The method is also suitable for determining SF values in case of "dirty" radionuclides (i.e., radionuclides that emit gamma rays in addition to positrons),[18] activity outside the FOV, and phantoms with deviating dimensions, as long as the exact dimensions are known.

In conclusion, as this method does not require measurements with special phantoms, it can be used to accurately